AIAA JOURNAL
Vol. 31, No. 7, July 1993

Accuracy of Flux-Split Algorithms in High-Speed Viscous Flows

Datta Gaitonde* and J. S. Shang†
Wright Laboratory, Wright-Patterson Air Force Base, Ohio 45433

The flux-vector split methods of MacCormack and Candler (MC) and of van Leer (vL) and the flux-difference split method of Roe are investigated in problems representative of complex flows under laminar conditions: the blunt-body flow at Mach 16 and the flow past a 24-deg compression corner at Mach 14. Higher order accuracy is obtained with the monotonic upwind-centered scheme for conservation laws (MUSCL) approach, viscous terms are centrally differenced, and an implicit relaxation method is employed for time integration. Emphasis is placed on evaluating the accuracy in prediction of surface quantities of engineering interest. The performance of the schemes is problem dependent. For the flow past the blunt body, the surface pressure is insensitive to the method as well as mesh resolution. Both the MC and Roe schemes predict accurate heat transfer rates whereas results with the vL method are dependent on the limiter employed. The overall distinction between the schemes is diminished for the compression corner especially on finer meshes. The extent of the separation region is notably influenced by the choice of the limiter. Several issues relating to the components of the calculation method are examined.

I. Introduction

A VARIETY of schemes have been proposed in the literature for the numerical representation of the inviscid fluxes in the Navier-Stokes equations. The more recent methods typically employ upwinding in one form or another to obtain algorithms possessing higher stability bounds and increased numerical efficiency. The inherently dissipative nature of upwind schemes is beneficial at or near shock waves where the inviscid fluxes dictate finite jumps in certain flow variables. However, typical *viscous* supersonic flows about bodies display steep gradients not only in regions with shocks but also in the boundary layers. The dissipative characteristics of upwind schemes in these latter regions are often a limitation since the numerical error may be comparable to or overwhelm the viscous terms. This can have detrimental consequences on the prediction of heat transfer rates.[1]

Upwind schemes may be classified according to the Riemann solver used to evaluate the fluxes at the cell faces and the procedure through which higher order spatial accuracy is obtained: monotonic upwind-centered scheme for conservation laws[2] (MUSCL) or non-MUSCL. The "symmetric" total variation diminishing (TVD) scheme of Yee and Harten as described in Ref. 3 and the "upwind" TVD scheme of Yee[3] are some examples of schemes obtaining higher order accuracy with non-MUSCL approaches.

The present research is focused on widely used MUSCL-based flux-split schemes. Specifically, we study the performance of 1) a modified version of the Steger-Warming scheme, hereafter referred to as the method of MacCormack and Candler[1] (MC), 2) the van Leer scheme[4] (vL), and 3) the Roe scheme based on the approximate Riemann solver of the same name.[5]

The popularity of these three flux-split methods in the computation of high-speed flows is likely to increase, especially with their extension to include high-temperature effects by several authors (e.g., Refs. 6 and 7). However, uniform comparisons of the relative merits of these schemes have been performed on either inviscid[8,9] or simple viscous flows.[10,11] An overall assessment of these methods based on the studies available in the literature is complicated by the ambiguity in specific implementation.

In this effort a detailed investigation is performed, with mesh resolution studies, of the prediction capabilities of those three algorithms on two viscous laminar problems with specific emphasis on the prediction of heat transfer rates. Details of each method are presented in Sec. II. The choice of problems and flow parameters is dictated by the need to simulate features generic to a wide range of complex flows for which reliable experimental data in the form of surface pressure and heat transfer are available.

1) Mach 16 blunt-body flow: Such flows are common in practical fluid dynamical applications. The relative simplicity of the flowfield permits a theoretical estimation of stagnation point heat transfer for validation purposes. Nevertheless, the simulation of blunt-body flows is often complicated by the occurrence of anomalous behavior that is generally manifested as the so-called "carbuncle" phenomenon.[12,13]

2) Mach 14 flow past a 24-deg compression ramp: The resultant flowfield, shown schematically in Fig. 1, exhibits the typical features encountered in strong viscous/inviscid interactions, such as occur generically in several situations, including in inlets and on control surfaces. The parameters chosen duplicate one of the experiments of Holden and Moselle.[14] The resultant flowfield is known to exhibit a large region of recirculation.[15]

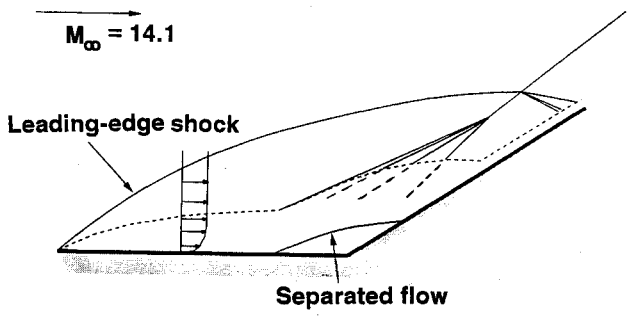

Fig. 1 Schematic of flow past 24-deg compression corner.

Received June 11, 1992; revision received Oct. 2, 1992; accepted for publication Oct. 2, 1992. This paper is declared a work of the U.S. Government and is not subject to copyright protection in the United States.

*Visiting Scientist, Flight Dynamics Directorate, WL/FIMM. Member AIAA.

†Senior Scientist, Flight Dynamics Directorate, WL/FIMM. Associate Fellow AIAA.

II. Theoretical Model

The two-dimensional Navier-Stokes equations in strong conservation form are solved in the transformed (ξ,η) coordinate plane:

$$\frac{\partial \tilde{U}}{\partial t}+\frac{\partial \tilde{F}}{\partial \xi}+\frac{\partial \tilde{G}}{\partial \eta}=0 \tag{1}$$

where $\tilde{U}$ is the solution vector of conserved variables $(\{\rho, \rho u, \rho v, \rho e\}/J)$ with ρ denoting density, u and v the Cartesian components of velocity, e the total energy per unit mass, and J the inverse cell volume. The variable e may further be expressed as $e_i + 0.5(u^2+v^2)$ with e_i denoting the internal energy per unit mass ($= C_v T$, where C_v is the specific heat at constant volume and T is the static temperature). The flux vectors $\tilde{F}$ and $\tilde{G}$ include the full viscous and inviscid terms. The density, static pressure p, and temperature are related through the equation of state $p=\rho RT$ where R is the gas constant. The molecular viscosity μ is approximated by Sutherland's law and the molecular Prandtl number Pr is assumed to be 0.73.

Equation (1) describes the balance of mass, momentum, and energy fluxes over an arbitrary control volume. On using the first-order Euler implicit formula and linearizing the fluxes in time, the discretized equation may be written in the following form[16]:

$$\{\text{NUMERICS}\}\ \delta\tilde{U} = \text{PHYSICS} \tag{2}$$

where PHYSICS represents the residual, NUMERICS is the implicit operator containing the flux Jacobians, and $\delta\tilde{U}$ denotes the change in the solution vector at each time step. The full Navier-Stokes equations are used in computing the residual with the appropriate upwind model for the inviscid terms, whereas viscous terms are evaluated in a centered fashion. Following Liou and van Leer,[17] the implicit operator employs the first-order Steger-Warming Jacobians to obtain strong diagonal dominance. The thin-layer approximation is invoked for the viscous Jacobians in the interest of simplicity. Time integration is achieved with a residual driven line Gauss-Seidel relaxation scheme as described in Refs. 16 and 18.

A brief description of the implementation of each scheme is presented with reference to the evaluation of the Cartesian flux G at a $j+\frac{1}{2}$ surface of the cell-centered finite volume formulation. The extension to general coordinates is straightforward.[8] The state of the flow at each interface is described by two vectors of conserved variables on either side, U^L and U^R. These are obtained by upwind extrapolation to the cell surface with the MUSCL approach of van Leer[2] in conjunction with a limiter. With W denoting the vector of extrapolated quantities,

$$W^L_{j+\frac{1}{2}} = W_j + \tfrac{1}{2}\tilde{\Delta}_{j+\frac{1}{2}}, \qquad W^R_{j+\frac{1}{2}} = W_{j+1} - \tfrac{1}{2}\tilde{\Delta}_{j+\frac{3}{2}} \tag{3}$$

where $\tilde{\Delta}$ introduces the limiter function f:

$$\tilde{\Delta}_{j+\frac{1}{2}} = f(\Delta_{j+\frac{1}{2}}, \Delta_{j-\frac{1}{2}}), \qquad \Delta_{j+\frac{1}{2}} = W^R_{j+\frac{1}{2}} - W^L_{j+\frac{1}{2}} \tag{4}$$

In the present work the primitive variables $(W = \{\rho\ u,\ v,\ p\})$ are extrapolated and U is then restored. The limiter f preserves monotonicity within the solution. Many limiter functions have been proposed in the literature. Most calculations in this work employ the minmod limiter[19] chosen for its popularity and robustness:

$$\begin{aligned} f(x, y) &= \text{minmod}(x, y) \\ &= \text{sgn}(x)\cdot\max\{0, \min[|x|, y\ \text{sgn}(x)]\} \end{aligned} \tag{5}$$

As shown later, the limiter is a crucial component of the overall algorithm, exerting a significant influence on the accuracy of the calculation. Other limiter formulas are presented in Sec. IV.

MacCormack and Candler Flux-Vector Split Algorithm

The formula for this scheme may be written as

$$G_{j+\frac{1}{2}} = B^{L+R/2}_{+}U^L + B^{L+R/2}_{-}U^R \tag{6}$$

Note that the same flow state $[(L+R)/2]$ is used to evaluate the positive and negative Jacobians $(B = \partial G/\partial U)$. This contrasts with the original Steger-Warming (SW) scheme,[20] in which the Jacobians are upwinded. MacCormack and Candler[1] proved that this simple modification results in a significant improvement in accuracy. The MC method was developed for application only in the boundary layers and in fact leads to numerical instability when applied at strong shock waves. In such regions, the scheme therefore reverts to the SW method in a smooth manner with a pressure-based switch described in Ref. 21.

van Leer Flux-Vector Split Algorithm

The functional form of the vL scheme is similar to that of the SW method. For supersonic flow, the formula is the same, whereas for subsonic flow, G was revised by van Leer to avoid the discontinuity exhibited by the SW scheme across sonic lines. The details of the method may be found in Ref. 4.

Roe's Flux-Difference Split Algorithm

The formula for this scheme reads

$$G_{j+\frac{1}{2}} = \tfrac{1}{2}[G(U^L) + G(U^R)] - \tfrac{1}{2}\hat{Q}\,|\hat{\Lambda}|\,\hat{Q}^{-1}(U^R - U^L) \tag{7}$$

where $Q\Lambda Q^{-1} = B$ and $\hat{}$ indicates evaluation at the Roe-averaged state between U^L and U^R.[5] Roe's scheme may violate the entropy condition when the eigenvalues at the Roe-averaged state vanish. Following Harten,[22] the eigenvalues $|\lambda|$ of $|A|$ are modified when they are below some small threshold δ:

$$|\lambda| = \frac{|\lambda^2+\delta^2|}{2\delta} \qquad |\lambda| < \delta \tag{8}$$

The value of δ is dependent on the grid as well as flow parameters. In the body-normal direction, an isotropic form is used[3]:

$$\delta = \tilde{\delta}J^{-1}[|\boldsymbol{u}\cdot\nabla\xi| + |\boldsymbol{u}\cdot\nabla\eta| + (c/2)(|\nabla\xi| + |\nabla\eta|)] \tag{9}$$

where $\tilde{\delta}$ is a specified constant. To prevent excessive dissipation due to the cell aspect ratio, the anisotropic cutoff formula described by Muller[23] is employed in the streamwise ξ direction:

$$\delta = \tilde{\delta}J^{-1}\lambda^{(\xi)}\left\{1+\left[\frac{\lambda^{(\eta)}}{\lambda^{(\xi)}}\right]^{\frac{2}{3}}\right\} \tag{10}$$

where $\lambda^{(k)} = |\boldsymbol{u}\cdot\nabla k| + c|\nabla k|$. For the flow past the compression ramp, the cutoff is applied only to the two nonlinear eigenvalues in each direction. For the blunt-body flow, however, it is necessary for the purpose of stability to apply the cutoff algorithm to the linear eigenvalue in the ξ direction as well.[24] The value of $\tilde{\delta}$ used is typically in the range of 0.05–0.1. Further discussion on the choice of the parameter $\tilde{\delta}$ is provided with the results.

III. Boundary Conditions and Numerical Details

For each flow, the boundaries may be categorized into one of the following. At an inflow boundary, the flow vector $\{\rho, \rho u, \rho v, \rho e\}$ is specified according to the known freestream state. At solid boundaries, the velocity vector and the normal pressure gradient are assumed zero and at a constant specified surface temperature. At outflow boundaries, the flow is predominantly supersonic and the zero gradient extrapolation condition is applied. The boundary conditions for the implicit portion of the formulation are applied by appropriate modification of the block matrices in Eq. (2).[16]

Convergence is determined for all computations by monitoring several quantities. The global residual (GR), defined as

$$\|\mathrm{GR}\| = \frac{1}{(IL)(JL)}\sqrt{\sum_{i=1}^{IL}\sum_{j=1}^{JL}\sum_{k=1}^{4}\left[\frac{(R_k)_{i,j}}{U_{\infty,k}}\right]^2} \tag{11}$$

is a reliable measure in these calculations. In Eq. (11), k denotes the kth component of U on an $IL \times JL$ computational mesh and $(R_k)_{i,j}$ is the change in the flow solution, $R_k = \Delta U_k$ at i,j and $U_\infty = \{\rho, \rho u, \rho u, \rho e\}_\infty$. Convergence is assumed when $\|\mathrm{GR}\|$ drops 8 or more orders of magnitude. In addition, the integrated root mean square (rms) pressure and heat transfer values over the entire surface are also monitored. At convergence, these assume constant values.

IV. Results

For the purposes of brevity, several results are stated without accompanying figures. The reader is referred to Ref. 21 for some of these details.

Blunt-Body Flow

The parameters for this flow are $M_\infty = 16.34$, cylinder radius = 0.038 m, $T_\infty = 52$ K, $p_\infty = 82.95$ N/m^2, Reynolds number = 3.94×10^6/m, and $T_{\text{wall}} = 294.4$ K. These represent a low enthalpy flow for which previous computations validate the perfect gas approximation.[25] Viscous calculations are performed on three grids (denoted 1, 2, and 3, respectively) described in Table 1. Each is generated by a combination of exponentially stretched and uniform spacings (Fig. 2). The most refined mesh (grid 3) satisfies the criteria of Klopfer and Yee,[26] who recommended a surface cell Reynolds number Re_c of roughly 3 for heat transfer calculations.

Calculations with each of the methods are compared with experimental values published by Holden et al.[27] The computed surface pressure is observed to be insensitive to mesh resolution for each scheme (not shown, see Ref. 21). The experimental surface pressure data exhibit significant scatter and are consistently lower than in the computations, an observation made previously by Prabhu et al.[25] The computed stagnation point pressure compares very well, however, with the results obtained from the Rayleigh supersonic pitot pressure formula, 2.9×10^4 N/m^2. In addition, the computed surface pressure values are independent of the particular scheme employed (not shown). This is perhaps a result of the fact that, in this instance, the surface pressure is dictated mainly by the shock strength and shape that in turn is accurately captured by all of the inviscid discretization methods at each level of mesh refinement. The shock is captured within at most two zones, and the shock standoff distance ($\Delta/R \sim 0.4$), defined with reference to the location of the sonic point, is invariant with respect to mesh resolution (not shown). On all schemes considered, this is indicative of the accuracy of computed bow shock strength and overall low conservation errors. Since these methods are based on one-dimensional Riemann solvers, the good alignment of the mesh with the shock wave may be an important factor. For reasons presented later, with Roe's scheme a higher value of the cutoff parameter $\bar{\delta}$ is necessary as the mesh is refined. Several calculations with different cutoff values ($0.4 < \bar{\delta} < 0.8$) indicate a negligible influence of this parameter on the computed surface pressure.

Figure 3 shows the computed surface heat transfer (in W/m^2) with the MC scheme. Overall, the agreement with experimental values is excellent even on the coarsest mesh, which has

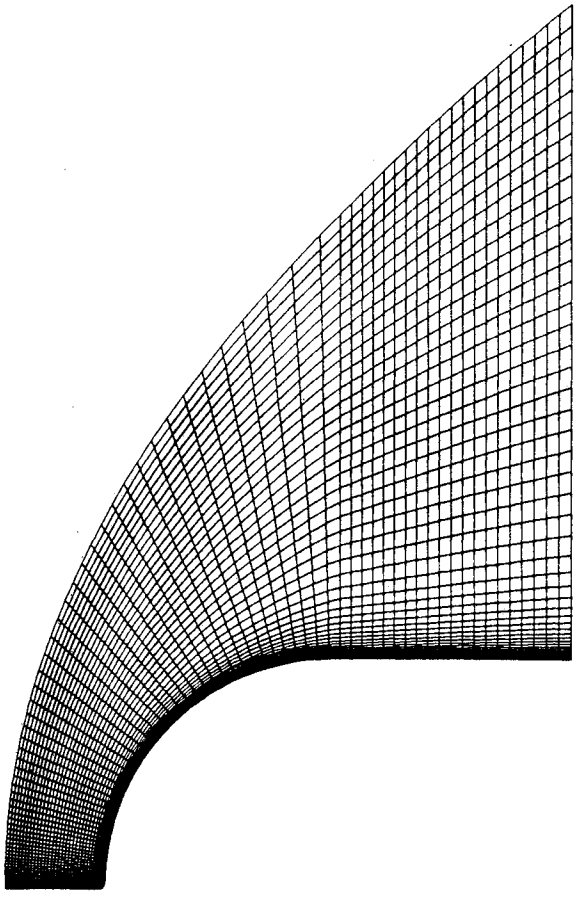

Fig. 2 Structure of mesh employed for blunt body.

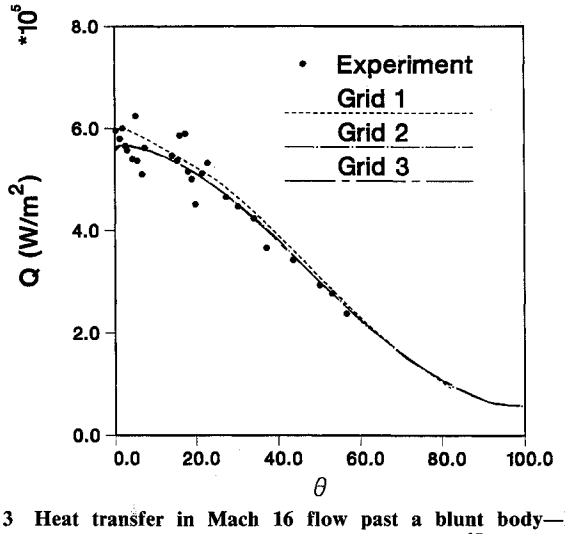

Fig. 3 Heat transfer in Mach 16 flow past a blunt body—MC scheme, minmod limiter (experiments of Holden et al.[27]).

Table 1 Blunt-body grid details[a]

Grid	$IL \times JL$	$Re_c\|_{\min}$	$Re_c\|_{\max}$	$Re_c\|_{\text{av}}$	$\Delta\theta\|_{\min}$	$\Delta\theta\|_{\max}$	$\Delta\theta\|_{\text{av}}$	$c\|_{\text{av}}$
1	19×17	19.4	125.3	51.5	1.10	10.5	6.6	1.98
2	39×35	8.1	51.6	20.6	0.51	5.3	3.4	1.41
3	79×71	3.7	24.2	9.6	0.25	2.5	1.7	1.18

[a] IL = points in ξ direction, JL = points in η direction, c = normal stretch factor at surface, $\Delta\theta$ = angular spacing in degrees, and Re_c = surface mesh Reynolds number based on half cell height in η direction.

a high surface cell Reynolds number and stretch factor (Table 1). The stagnation heat transfer value compares very well with that predicted theoretically by Fay and Riddell[28] of 5.6×10^5 W/m^2. Results from the SW method (not shown for the purposes of brevity) indicate an overprediction in heat transfer of 500, 400, and 250%, respectively, on grids 1, 2, and 3. Thus, the MC method, proposed as a correction to the SW scheme, is a significant improvement. However, the former exhibits a tendency to develop the anomalous carbuncle solution, whereas the latter does not. This represents a limitation of the switching algorithm that reverts the MC method to the SW method near shocks. For the displayed results, the carbuncle problem is eliminated by explicitly applying the SW scheme at a few points on either side of the shock, i.e., overriding the pressure-based switch mentioned earlier.

In sharp contrast to the MC scheme, the vL method exhibits a drastic effect of grid resolution on the heat transfer rates (Fig. 4). Despite the accurate shock representation, heat transfer rates on the coarse mesh are overpredicted by a large amount over the entire surface (120% over the theoretical value at the stagnation point). The accuracy improves notably with increased grid resolution: 52 and 15% overpredictions are observed on grids 2 and 3, respectively. These results indicate the extreme diffusiveness of the vL scheme when employed as presented in Sec. II.

An effort is made to improve the accuracy of the predicted heat transfer by modification of some aspects of the implementation. The effect of considering different sets of variables in the extrapolated vector W is examined by the different choices $W = \{\rho, \rho u, \rho v, p\}$ and $\{\rho, \rho u, \rho v, \rho e\}$. A limited examination on grid 2 reveals no significant influence on the accuracy of the final result (not shown). The second element examined is the choice of limiter that can affect both the robustness as well as the accuracy of the overall algorithm. In addition to the minmod limiter of Eq. (5) (denoted limiter 1), two others proposed by van Leer (limiter 2) and van Albada (limiter 3) are investigated[19]:

Limiter 2:

$$f(x, y) = \frac{x \cdot y + |x \cdot y|}{x + y + \epsilon} \tag{12}$$

Limiter 3:

$$f(x, y) = \frac{x \cdot (y^2 + \epsilon) + y \cdot (x^2 + \epsilon)}{x^2 + y^2 + 2 \cdot \epsilon} \tag{13}$$

where ϵ is a small number to prevent division by zero. Heat transfer results on the surface with grid 1 are presented in Fig.

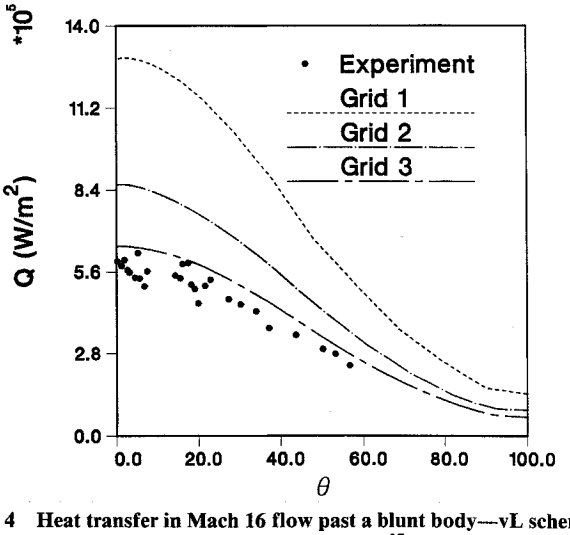

Fig. 4 Heat transfer in Mach 16 flow past a blunt body—vL scheme, minmod limiter (experiments of Holden et al.[27]).

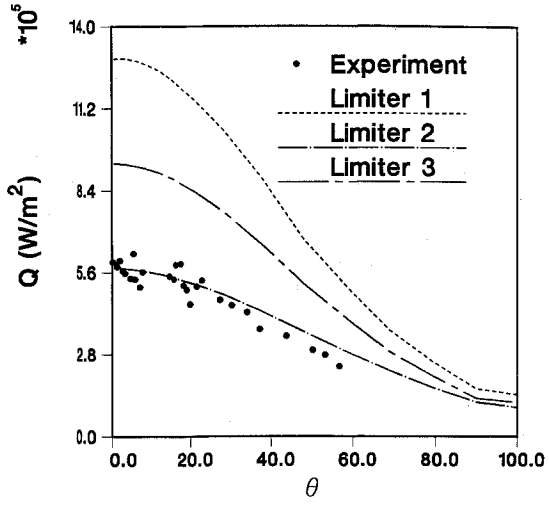

Fig. 5 Influence of limiter on heat transfer rates with vL scheme on grid 1 (experiments of Holden et al.[27]).

5, which illustrates clearly the strong dependence of the computed heat transfer on the limiter. Indeed, on grid 1, the vL scheme in conjunction with limiter 2 is comparable in accuracy to the other two schemes that do not exhibit a similar sensitivity to choice of limiter. With increased grid resolution, limiter 2 retains its accuracy, whereas results with limiter 3 improve to closer agreement with experimental values. Although these limiters provide higher accuracy than minmod, there is an associated loss of robustness. The global residual exhibits only 5 orders of magnitude reduction though the solution converges in the surface rms quantities.

Turning to Roe's scheme, previous research[12,13] has highlighted a tendency toward the development of the carbuncle for blunt-body flows. In the present work, two practical approaches are discussed for the suppression of this behavior.

In the first approach, the value of the constant $\bar{\delta}$ in the entropy correction formula [Eqs. (9) and (10)] is increased until the anomalies disappear. Under these conditions, the overall accuracy of this scheme is comparable to that of the MC method. Consequently, the surface heat transfer profiles for each of the calculations discussed later are similar to those presented in Fig. 3 and are not repeated. For grid 1, no carbuncle is observed even for very small values of $\bar{\delta}$ used (0.05). The truncation error provided by the coarseness of this mesh is possibly sufficient to stabilize the calculation. For grid 2, anomalous solutions are detected as carbuncles in the Mach contours (not shown) at small values of $\bar{\delta}$. On increasing $\bar{\delta}$ to 0.3, all evidence of the carbuncle disappears. Further increase to 0.4 has no observable effect at the surface. Although a rigorous examination of the minimum value allowable for an anomaly free solution is not attempted, for grid 3 the strategy followed is to increase $\bar{\delta}$ in increments of 0.1 until all evidence of anomaly disappears in the flow variables. A minimum value of 0.5 is required. Further increase up to $\bar{\delta} = 0.8$ has only a modest effect on the computed surface quantities. Clearly, higher values of the cutoff parameter stabilize the calculations with no conspicuous penalty. However, there is evidence that this is not the case in other, more complex flowfields, e.g., the type IV shock-shock interaction.[21]

The second approach to the problem takes recourse to the fact that other splittings, such as SW or vL, exhibit no carbuncle. Although the preceding discussion highlights the prohibitively dissipative nature of these schemes in the boundary layer, a compromise is achieved by using a combination of splittings: in the streamwise direction SW or vL is employed, whereas in the body normal direction the unmodified higher order Roe scheme is retained. This approach is indeed successful in suppressing the carbuncle. Heat transfer results for grids 1 and 2 are shown in Fig. 6 for different streamwise splittings.

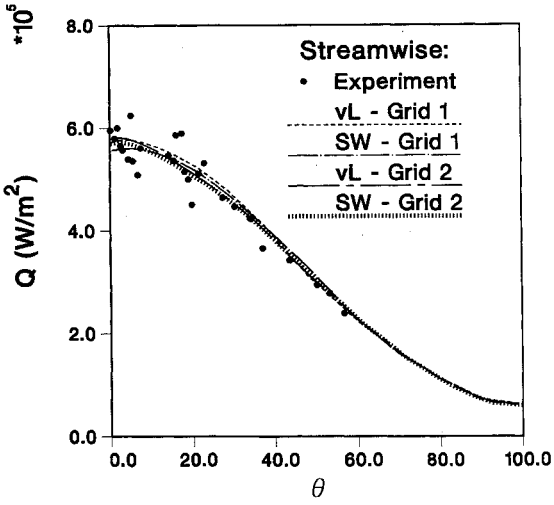

Fig. 6 Effect of different streamwise splittings on computed heat transfer—Roe's scheme in the body normal direction, minmod limiter (experiments of Holden et al.[27]).

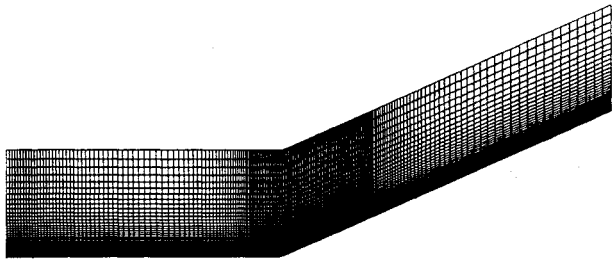

Fig. 7 Structure of grids 1, 2, and 3 for compression corner.

There is no significant degeneration in accuracy in comparison with the scheme employing Roe's method in both directions. These results suggest that the surface characteristics of such blunt-body flowfields are primarily dependent on the scheme employed in the direction normal to the body. The streamwise method may therefore be chosen based on the numerical stability considerations.

Corner Flow

The parameters for this flow simulate the experimental evidence of Holden and Moselle[14]: $M_\infty = 14.1$, ramp angle = 24 deg, $T_\infty = 72.7$ K, $p_\infty = 10.1$ N/m^2, Reynolds number = 2.4×10^5/m, and $T_{wall} = 297.22$ K. In a recent study, Rudy et al.[15] examined this flowfield with several different codes and concluded that calculation methods require the incorporation of three-dimensional effects for accurate comparison with experimental data. Their results, as well as those of Rizzetta and Mach,[29] indicate a larger extent of separation region than observed experimentally when three-dimensional influences are neglected. These findings introduce an element of uncertainty in the estimation of accuracy of the schemes under examination. Hence, the present results are first compared with experiment and then related to the calculations of other researchers.

Two types of meshes are considered for this study: grids 1, 2, and 3 are simply sheared (Fig. 7), exponentially stretched on either side of the interaction and also in the surface normal direction. Grid 4 addresses the issue of leading-edge shock resolution by including a small portion of the flow upstream. In addition, a higher mesh density is afforded in the vertical direction through an appropriate redefinition of the domain (Fig. 8). The characteristics of the grids used are presented in Table 2. The mesh density of grid 4 is comparable to that of the 101×101 mesh on which grid independent results were obtained by Rudy et al.[15]

The results are discussed principally with reference to the comparison with experiment of the computed pressure, heat transfer, and skin friction coefficients. Attention is focused on the magnitudes and locations of peak values in each, as well as the extent of the interaction.

Overall, the effect of increased grid resolution offered by grids 1–3 provides better comparison between theory and experiment with all methods. However, no conspicuous differences are observed in the computed quantities between grids 3 and 4. For this common horizontal mesh spacing, therefore, the vertical resolution of grid 3 is deemed sufficient, and leading-edge resolution effects are negligible. Only figures pertaining to grid 4 are included for conciseness.

On the coarser meshes, grids 1 and 2, the initial pressure rise occurs close to the corner, far downstream of the experimental value (not shown). The peak pressure exceeds the inviscid rise as a result of the viscous-inviscid interaction but is, however, underpredicted. Figure 9 presents the comparison of pressure coefficient, defined as $2(p_w - p_\infty)/\rho_\infty u_\infty^2$, with the MC, vL, and Roe schemes, respectively, on grid 4. The abscissa is the streamwise distance normalized by the distance from the leading edge to the corner ($L = 0.44$ m). The figure is also representative of the calculation on grid 3. The pressure coefficient

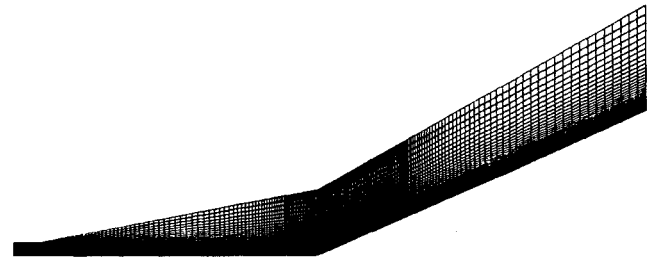

Fig. 8 Structure of grid 4 for compression corner.

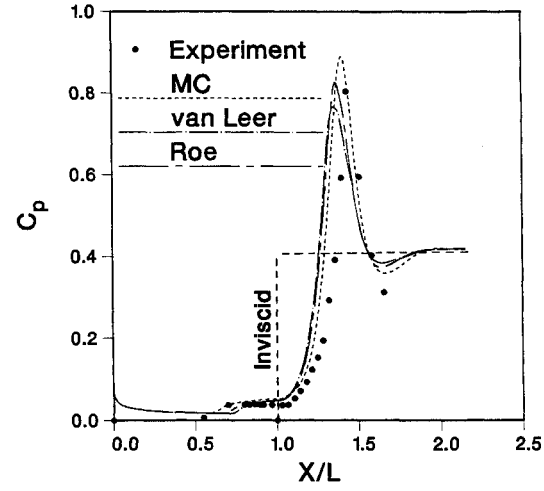

Fig. 9 Comparison of pressure coefficient for compression corner flow—grid 4, minmod limiter (experiments of Holden and Moselle[14]).

Table 2 Compression corner grid details[a]

Grid	$IL \times JL$	$Re_c\|_{av}$	$\Delta x\|_{min}$	$\Delta x\|_{max}$	$\Delta x\|_{av}$	$c\|_{av}$
1	49×14	47.6	0.02	0.12	0.04	1.4
2	99×29	21.7	0.01	0.06	0.02	1.2
3	199×59	10.3	0.005	0.03	0.01	1.1
4	209×59	5.9	0.005	0.03	0.01	1.1

[a] IL = points in ξ direction, JL = points in η direction, c = normal stretch factor at surface, $\Delta\theta$ = angular spacing in degrees, and Re_c = surface mesh Reynolds number based on half cell height in η direction.

exhibits relatively larger differences between the methods than observed for the blunt-body calculation. The initial pressure rise occurring at about $x/L \sim 0.6$ is best reproduced by the MC method. For the Roe and van Leer schemes, this increase occurs slightly downstream nearer the corner ($x/L \sim 0.75$), resulting in a smaller separation region as discussed later. The location of the peak pressure is also best predicted with the MC method, although the magnitude is about 12% larger than in the experiment. With the vL and Roe schemes, the computed peak falls slightly upstream of the experimental value, whereas the magnitude is quite accurate in comparison with experiment. For each mesh, the theoretical inviscid pressure asymptote is reached beyond $x/L \sim 2$.

The heat transfer results on grid 4 are displayed in Fig. 10. The ordinate in this figure is the heat transfer coefficient defined as $k(\partial T/\partial n)_w/\rho_\infty u_\infty(H_0 - H_w)$, where H is the total enthalpy, and the subscript w denotes evaluation at the wall. It is evident that the MC method predicts the initial drop at the correct location, whereas the Roe and vL schemes underpredict upstream influence. On the other hand, the least discrepancy in peak heating value is obtained with Roe's scheme (15% overprediction). Higher values in C_h result with the MC method (30% overprediction).

Figure 11 compares the calculated skin friction coefficient, defined as $2\mu_w(\partial u/\partial n)_w/\rho_\infty u_\infty^2$. The size of the separated reverse flow region is evident from the range of negative skin

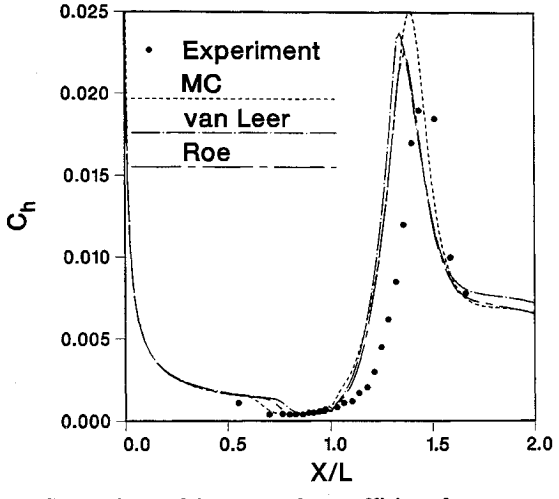

Fig. 10 Comparison of heat transfer coefficient for compression corner flow—grid 4, minmod limiter (experiments of Holden and Moselle[14]).

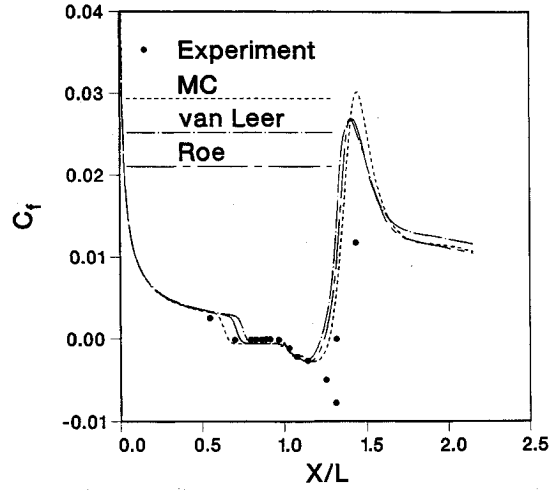

Fig. 11 Comparison of skin friction coefficient for compression corner flow—grid 4, minmod limiter (experiments of Holden and Moselle[14]).

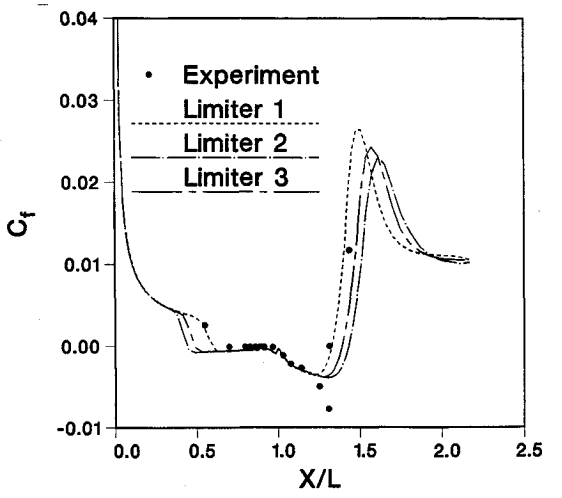

Fig. 12 Effect of limiter on skin friction coefficient—Roe scheme, grid of Rudy et al.[15] (experiments of Holden and Moselle[14]).

friction values. All methods indicate negligible separation on grid 1 as a result of a lack of adequate resolution of the viscous terms (not shown). For grids 3 and 4, the predictions with the vL method approach those of the other two schemes, a trend also observed earlier with the heat transfer. The most accurate onset of the separation region in comparison with experimental values is obtained with the MC scheme. All three methods fail, however, to correctly estimate the magnitude of drop in skin friction coefficient at $X/L \sim 1.25$, i.e., near the flow reattachment.

It is interesting to note that, although the vL scheme performs poorly on the coarser meshes, significant improvement is obtained with grid refinement in the prediction of surface quantities. Unlike in the blunt-body instance where it was observed to be highly diffusive with the minmod limiter, the method is clearly comparable to the other two for this flow, especially on the finer meshes. The precise locations of separation and reattachment points as well as the extent of the separation region are provided in Ref. 21.

Although detailed comparison with the calculations of other researchers is not possible due to differences in implementations and mesh details, the results presented earlier differ in some respects from those of other efforts. In particular, the Computational Fluids Laboratory 3-D (CFL3D) code, using Roe's scheme with a third-order procedure and the thin-layer approximation for the viscous terms, has been applied to the same configuration by Rudy et al.[15] Their results indicate very good agreement with experimental data on a relatively coarse mesh (51×51). However, further increased mesh resolution leads to a larger separated region than that observed experimentally. To examine the cause of this discrepancy with the present computations, attention is focused on Roe's scheme and the 101×101 mesh used (and made available for this work) by Rudy et al.[15]

Two elements of the theoretical framework are examined: 1) the magnitude of the cutoff parameter and 2) the choice of the limiter function. The effect of the cutoff parameter on the computed solution is negligible (not shown). This conclusion is based on calculations with $\tilde{\delta}$ values of 0.05, 0.01, and 0.00 (no cutoff) that exhibit only minor discrepancies with the results presented previously with Roe's scheme on grid 4 (see Figs. 9–11). These may be attributed to differences in detailed grid structure. The mesh of Rudy et al.[15] has a coarser spacing near the wall than grid 4 but has more points and a smaller stretch factor in the vertical direction. Consequently, better resolution is achieved of the shock structure in the viscous-inviscid interaction region above the corner.

The influence of the limiter is more drastic and brings the present results in closer agreement with those of Rudy et al.[15] Figure 12 exhibits the computed skin friction coefficient with

$\tilde{\delta} = 0$ and the three limiters presented earlier. The solution is clearly sensitive to the choice of limiter. Limiters 2 and 3 predict larger separation regions than minmod as a consequence of upstream movement of the point of separation coupled with a downstream motion of the point of reattachment. These limiters also exhibit lower values of peak skin friction coefficient at a location further downstream. A similar trend is observed in the pressure and heat transfer coefficients (not shown). These results reaffirm the importance of the limiter in such high-speed complex interactions. Further work is necessary to resolve these issues.

V. Conclusions

A detailed examination of the performance of several flux-split algorithms is attempted on problems representative of complex flowfields. Results are compared with experimentally observed data. Although these schemes were developed primarily for use in inviscid flows, their accuracy in predicting quantities of engineering interest in viscous flows with complex features is encouraging but dependent on the configuration under examination. For the Mach 16 blunt-body flow, inviscid dominated phenomena such as shock strength and standoff distance are equally well predicted with all schemes. Both the scheme of MacCormack and Candler and Roe's method show comparably good ability to predict accurate heating rates even on relatively coarse meshes, whereas van Leer's method is sensitive to the limiter employed. Techniques are suggested to suppress anomalous carbuncle solutions with reference to Roe's scheme. In the flow past the compression corner, the distinction between the three schemes is more pronounced in surface pressure but less so in heat transfer rates and skin friction. All three methods underpredict the skin friction trough near reattachment even on the finest mesh computed. The flow details, including the size of the predicted separation region, are dependent on the limiter.

Acknowledgments

The computer support offered by Wright-Patterson Air Force Base and the Numerical Aerodynamic Simulation program is gratefully acknowledged. The authors wish to thank P. G. Huang for several inspiring discussions, especially on limiters. The assistance of D. Rizzetta in grid development is appreciated as is D. Rudy's permission to use the 101×101 mesh.

References

[1]MacCormack, R. W., and Candler, G. V., "The Solution of the Navier-Stokes Equations Using Gauss-Seidel Line Relaxation," *Computers and Fluids,* Vol. 17, No. 1, 1989, pp. 135–150.

[2]van Leer, B., "Towards the Ultimate Conservation Difference Scheme V, A Second-Order Sequel to Godunov's Method," *Journal of Computational Physics,* Vol. 32, No. 1, 1979, pp. 101–136.

[3]Yee, H. C., "Upwind and Symmetric Shock-Capturing Schemes," NASA TM-89464, May 1987.

[4]van Leer, B., "Flux-Vector Splitting For the Euler Equations," Inst. for Computer Applications in Science and Engineering, ICASE Rept. 82-30, Hampton, VA, Sept. 1982.

[5]Roe, P. L., "Approximate Riemann Solvers, Parameter Vectors and Difference Schemes," *Journal of Computational Physics,* Vol. 43, No. 2, 1981, pp. 357–372.

[6]Liu, Y., and Vinokur, M., "Nonequilibrium Flow Computations: I. An Analysis of Numerical Formulation of Conservation Laws," *Journal of Computational Physics,* Vol. 83, No. 2, 1989, pp. 373–397.

[7]Grossman, B., and Cinnella, P., "Flux-Split Algorithms for Flows with Nonequilibrium Chemistry and Vibrational Relaxation," *Journal of Computational Physics,* Vol. 88, No. 1, 1990, pp. 131–168.

[8]Anderson, W. K., Thomas, J. L., and van Leer, B., "A Comparison of Finite Volume Flux Vector Splittings for the Euler Equations," AIAA Paper 85-0122, Jan. 1985.

[9]Kroll, N., Gaitonde, D., and Aftosmis, M., "A Systematic Comparative Study of Several High Resolution Schemes for Complex Problems in High Speed Flows," AIAA Paper 91-0636, Jan. 1991.

[10]van Leer, B., Thomas, J. L., Roe, P. L., and Newsome, R. W., "A Comparison of Numerical Flux Formulas for the Euler and Navier-Stokes Equations," AIAA Paper 87-1104, June 1987.

[11]von Lavante, E., "Accuracy of Upwind Schemes Applied to the Navier-Stokes Equations," *AIAA Journal,* Vol. 28, No. 7, 1990, pp. 1312–1314.

[12]Peery, K. M., and Imlay, S. T., "Blunt-Body Flow Simulations," AIAA Paper 88-2904, July 1988.

[13]Liou, M.-S., and Steffen, C. J., Jr., "Development of New Flux Splitting Schemes," *CFD Compendium of Abstracts, Computational Fluid Dynamics Conference,* NASA Ames Research Center, March 1991.

[14]Holden, M. S., and Moselle, J. R., "Theoretical and Experimental Studies of the Shock Wave-Boundary Layer Interaction on Compression Surfaces in Hypersonic Flow," Rept. ARL 70-0002, Wright-Patterson AFB, OH, Jan. 1970.

[15]Rudy, D. H., Thomas, J. L., Kumar, A., Gnoffo, P. A., and Chakravarthy, S. R., "Computation of Laminar Hypersonic Compression-Corner Flows," *AIAA Journal,* Vol. 29, No. 7, 1991, pp. 1108–1113.

[16]MacCormack, R., "Current Status of Numerical Solutions of the Navier-Stokes Equations," AIAA Paper 85-0032, Jan. 1985.

[17]Liou, M.-S., and van Leer, B., "Choice of Implicit and Explicit Operators for the Upwind Differencing Method," AIAA Paper 88-0624, Jan. 1988.

[18]Thomas, J. L., and Walters, R. W., "Upwind Relaxation Algorithms for the Navier-Stokes Equations," AIAA Paper 85-1501, July 1985; also *AIAA Journal,* Vol. 25, No. 4, 1987, pp. 527–534.

[19]Yee, H. C., Klopfer, G. H., and Montagne, J.-L., "High-Resolution Shock-Capturing Schemes for Inviscid and Viscous Hypersonic Flows," NASA TR 100097, April 1988.

[20]Steger, J. L., and Warming, R. F., "Flux Vector Splitting of the Inviscid Gasdynamic Equations with Application to Finite Difference Methods," *Journal of Computational Physics,* Vol. 40, No. 2, 1981, pp. 263–293.

[21]Gaitonde, D. V., and Shang, J. S., "The Performance of Flux-Split Algorithms in High-Speed Viscous Flows," AIAA Paper 92-0186, Jan. 1992.

[22]Harten, A., "High Resolution Schemes for Hyperbolic Conservation Laws," *Journal of Computational Physics,* Vol. 49, No. 3, 1983, pp. 357–393.

[23]Muller, B., "Simple Improvements of an Upwind TVD Scheme for Hypersonic Flow," AIAA Paper 89-1977, June 1989.

[24]Riedelbauch, R., and Brenner, G., "Numerical Simulation of Laminar Hypersonic Flow Past Blunt Bodies Including High Temperature Effects," AIAA Paper 90-1492, June 1990.

[25]Prabhu, R. K., Stewart, J. R., and Thareja, R. R., "A Navier-Stokes Solver for High Speed Equilibrium Flows and Application to Blunt Bodies," AIAA Paper 89-0668, Jan. 1989.

[26]Klopfer, G. H., and Yee, H. C., "Viscous Hypersonic Shock-On-Shock Interaction on Blunt Cowl Lips," AIAA Paper 88-0233, Jan. 1988.

[27]Holden, M. S., Wieting, A. R., Moselle, J. R., and Glass, C., "Studies of Aerothermal Loads Generated in Regions of Shock/Shock Interaction in Hypersonic Flow," AIAA Paper 88-0477, Jan. 1988.

[28]Fay, J., and Riddell, F., "Theory of Stagnation Point Heat Transfer Rate in Dissociated Air," *Journal of the Aeronautical Sciences,* Vol. 25, No. 2, 1958, pp. 73–85.

[29]Rizzetta, D. P., and Mach, K. D., "Comparative Numerical Study of Hypersonic Compression Ramp Flows," AIAA Paper 89-1877, June 1989.